Surface Heat Flux in the East China Sea and the Yellow Sea

NAOKI HIROSE

Interdisciplinary Graduate School of Engineering Sciences, Kyushu University, Kasuga, Japan

HYUN-CHUL LEE* AND JONG-HWAN YOON

Research Institute for Applied Mechanics, Kyushu University, Kasuga, Japan

(Manuscript received 12 March 1997, in final form 19 March 1998)

ABSTRACT

Climatological monthly mean variations of the surface heat fluxes over the East China Sea and the Yellow Sea are calculated by both a data analysis and a numerical simulation. The result of the data analysis based on the empirical/bulk method agrees well with the directly observed solar radiation and several previous studies of the surface heat fluxes. An adjustment in the formation of the Haney-type heat flux is presented by comparing to the result of the bulk method. The numerical simulation of these seas using an ocean general circulation model demonstrates the success of the improved Haney-type condition over the original one in simulating sea surface temperature. The surface heat flux simulated in the Yellow Sea is more reasonable than by the data analysis considering the total heat budget of this sea.

1. Introduction

The East China Sea (ECS) and the Yellow Sea (YS) are marginal seas located in the northwestern part of the Pacific. These seas are surrounded by the Eurasian continent, Korean Peninsula, Japanese islands, and Taiwan Island as shown in Fig. 1. The continental shelf shallower than 200 m occupies about 80% of the area. The water masses on the shelf region are greatly affected by the air–sea heat exchange. We can even observe the sea ice formation in the northern end of the Sea of Bohai. On the other hand, the Kuroshio flows along the continental slope in ECS, and a strong heat loss occurs from sea to air, especially in winter (Kondo 1976). These seas represent the large variation of the heat budget. A quantitative analysis of the heat fluxes as well as the qualitative one should be carried out to understand the formation and modification of water masses.

The Air Mass Transformation Experiments (AMTEX) were carried out during February 1974 and 1975 in the ECS. Kondo (1976) first reported on the heat balance of the ECS and YS as a result of AMTEX. He showed that the total heat loss along the Kuroshio and in the sea near the Chinese mainland is about 350 and 100 W m^{-2} during these periods, respectively.

Recently, several studies have reported on the surface heat fluxes all over the ECS and YS based on the bulk method using a large amount of data (Ishii and Kondo 1987; Sakurai et al. 1989; Kim 1992; Kang et al. 1994). However, the results show inconsistencies among them, as will be shown later. The limitation or inaccuracy of the data and uncertain empirical formulae might cause these disparities.

In order to estimate a reliable surface heat budget, we calculate the heat fluxes across the sea surface using a data analysis based on the bulk method and a numerical simulation of the ocean circulation. The accuracy of the data analysis in this study will be the same order of the recent studies because the data and methodology of this study are very different from them, but the numerical simulation will supply the physically corrected heat flux especially in the data-poor regions.

Surface net heat flux is often given by a restoring condition such as that of Haney (1971) or Barnier et al. (1995). The accuracy of the thermal forcing depends not only on the restoring quantity (air or sea surface temperature, etc.) but also on the damping coefficients. We seek more accurate coefficients in the formation of the Haney-type surface thermal boundary condition, and

* Current affiliation: Programs in Atmospheric and Oceanic Sciences, Princeton University, Princeton, New Jersey.

Corresponding author address: Mr. Naoki Hirose, ESST, Kyushu University, 6-1 Kasuga-Kouen, Kasuga, Fukuoka 816-8580, Japan. E-mail: nick@riam.kyushu-u.ac.jp

reestimate the surface heat flux by simulating the ocean circulation of the ECS and YS.

In the next section, we analyze the surface heat flux based on the bulk method and calculate a Haney-type heat flux for the numerical model. In section 3, the numerical simulation is carried out with an ocean general circulation model (OGCM). The last section gives the summary and discussions.

2. Analysis of observed data

a. Formulation

The net heat flux through the sea surface Q_{net} can be expressed as

$$Q_{\text{net}} = Q_s - (Q_b + Q_h + Q_e), \tag{1}$$

where Q_s and Q_b are the short- and longwave radiation fluxes and Q_h and Q_e are the sensible and latent heat fluxes, respectively. Each component of the heat fluxes is calculated by the empirical formulas in this study:

$$Q_s = I_0(0.865 - 0.5C^2)(1 - \alpha_s) \tag{2}$$

$$Q_b = \varepsilon\sigma\theta_a^4(0.254 - 0.00495e_a)(1 - \delta C) + 4\varepsilon\sigma\theta_a^3(T_s - T_a) \tag{3}$$

$$Q_h = \rho_a c_a c_h (T_s - T_a)W \tag{4}$$

$$Q_e = \rho_a L c_e (q_s - q_a)W. \tag{5}$$

The meanings of the variables and constants in these formulas are summarized in Table 1. Equations (2) and (3) were proposed by Kim and Kimura (1995) and Efimova (1961), respectively. The bulk transfer coefficients (c_h and c_e) of Kondo (1975) are adopted for (4) and (5). These schemes are chosen according to Kim and Kimura (1995). They evaluated various bulk and empirical formulas by comparison to direct observations and concluded the above four formulas are the most precise ones for the neighboring seas around Japan. Direct heat transport by precipitation and rivers is assumed to be negligible.

Haney (1971) proposed a simple formula of the net heat flux:

$$Q_{\text{net}} \approx Q_{\text{net}}(T_a) - \left(\frac{\partial Q_{\text{net}}}{\partial T_s}\right)_{T_a}(T_a - T_s) \tag{6}$$

$$= Q_1 + Q_2(T_a - T_s) \tag{7}$$

as a surface thermal boundary condition for the modeling of the ocean circulation. This formation can be recognized as a truncated Taylor expansion of the net heat flux. The quantities Q_1 and Q_2 are obtained from the following equations:

$$\begin{aligned} Q_1 &= Q_{\text{net}}(T_a) \\ &= Q_s(T_a) - (Q_b(T_a) + Q_h(T_a) + Q_e(T_a)) \\ &= I_0(0.865 - 0.5C^2)(1 - \alpha_s) - \varepsilon\sigma\theta_a^4(0.254 - 0.00495e_a)(1 - \delta C) + 0 - \rho_a L c_e (q_s(T_a) - q_a)W \end{aligned} \tag{8}$$

$$\begin{aligned} Q_2 &= -\left(\frac{\partial Q_{\text{net}}}{\partial T_s}\right)_{T_a} \\ &= -\left(\frac{\partial Q_s}{\partial T_s}\right)_{T_a} + \left(\frac{\partial Q_b}{\partial T_s}\right)_{T_a} + \left(\frac{\partial Q_h}{\partial T_s}\right)_{T_a} + \left(\frac{\partial Q_e}{\partial T_s}\right)_{T_a} \\ &= 0 + 4\varepsilon\sigma\theta_a^3 + \rho_a c_p c_h W + \rho_a L c_e W \frac{\epsilon}{P_a}\frac{0.031532}{(1 + 0.00412T_a)^2} e_s(T_a)\ \ln 10. \end{aligned} \tag{9}$$

We assumed in this calculation that the bulk coefficients c_h and c_e are approximately independent on T_s. In the numerical models, T_a is usually substituted by the climatological mean air temperature and T_s is regarded as T_1, which is the simulated water temperature at the first level below the sea surface. As shown in (8) and (9), the quantities Q_1 and Q_2 include much information of the meteorological values except the air–sea temperature difference ($T_a - T_s$). Therefore, we consider the quantities should vary in time and space.

b. Data source

Figure 1 shows the area of present analysis. The dimensions of the ECS and YS are 8.09×10^5 and 4.62×10^5 km^2, respectively. The Sea of Bohai is treated as the northwestern part of the YS in this study. The duration of the analysis is 31 yr from 1960 to 1990 (a total of 372 months).

The following three datasets are used in this study: COADS (Comprehensive Ocean–Atmosphere Data Set) CMR.5 files, NODC (National Oceanographic Data

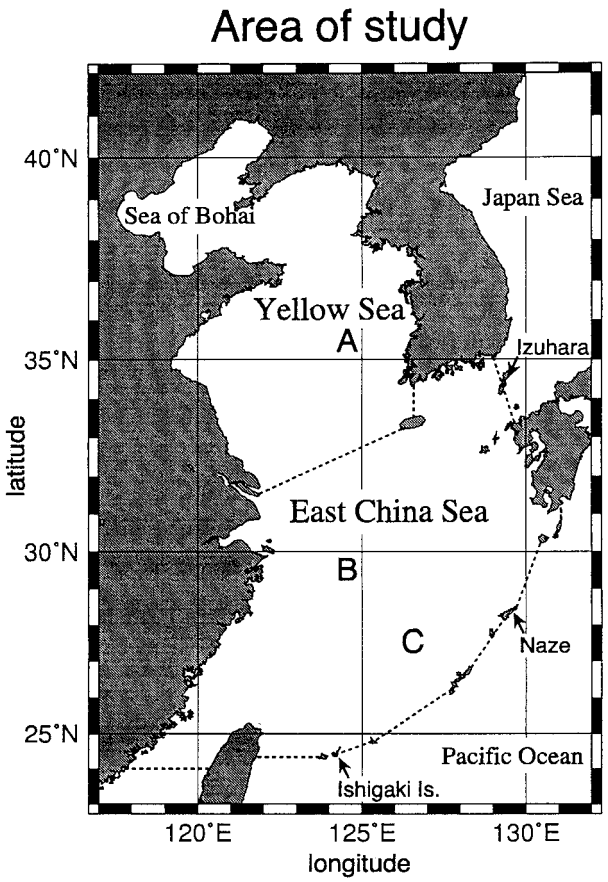

FIG. 1. Map of the study area. Quantitative comparison to the previous studies is carried out at the three positions A, B, and C.

Center) Oceanographic Station Data (SD2), and JODC (Japan Oceanographic Data Center) ship reports. The data from COADS occupy about 95% of all. The individual observation includes six marine meteorological quantities (T_a, T_s, e_a, C, W, P_a), which are required to compute the surface heat fluxes by the bulk method. Here P_a is the air pressure, which is needed to calculate the specific humidity. Any missing data of the former five components are not used in this study. In case of missing data P_a is only assumed to be 1013 hPa.

The number of qualified data at each 1° square is shown in Fig. 2. The method of quality control will be described in section 2c. The total number of data is 282 369 for the ECS and 16 131 for the YS. The amount of data is sufficient to obtain climatological means in the ECS and the southern part of the YS, but observations are sparse in the northern and the western part of the YS. The estimated flux in this area will be erroneous.

Figure 3 shows the time series of the observation frequencies in month for the analysis period. It can be clearly seen that observations have been carried out frequently in the ECS; however, very few data are obtained for the YS in the early 1970s. The limitation of the data in the YS has been a serious problem in the previous studies (Ishii and Kondo 1987; Sakurai et al. 1989).

c. Process of analysis

The quality control is carried out to remove extraordinary values of data as follows:

1) The duplicated data are removed.
2) The data located on land are excluded.
3) Abnormal values are removed using the following criteria:

$$\left.\begin{array}{ll} T_s \le -5.0°\text{C}, & 35.0°\text{C} \le T_s \\ T_a \le -70.0°\text{C}, & 70.0°\text{C} \le T_a \\ e_a < 0.0 \text{ hPa}, & 100.0 \text{ hPa} \le e_a \\ C < 0.0, & 1.0 < C \\ W < 0.0 \text{ m s}^{-1}, & 100.0 \text{ m s}^{-1} \le W \end{array}\right\}. \quad (10)$$

4) The values beyond 3.0 standard deviations from the

TABLE 1. Values of the variables and constants in (2)–(5): I_0 and δ are referred to in Seckel and Beaudry (1973), Reed (1977), and Berliand and Berliand (1952).

Parameter	Symbol	Value
Solar radiation under clear sky	I_0	W m^{-2}
Amount of cloud	C	0–1 (−)
Albedo at the sea surface	α_s	0.06 (−)
Emissivity at the sea surface	ε	0.97 (−)
Stefan–Boltzmann constant	σ	5.6705×10^{-8} W m^{-2} K^{-4}
Air temperature	T_a, θ_a	°C, K
Sea surface temperature	T_s	°C
Vapor pressure	e_a	hPa
Cloud coefficient	δ	0.60–0.69 (−)
Air density	ρ_a	1.290–1.305 kg m^{-3}
Specific heat of air	c_a	1004.6 J kg^{-1} °C^{-1}
Bulk transfer coefficients	c_h, c_e	(−)
Wind speed	W	m s^{-1}
Latent heat of evaporation	L	2.50–2.57 J kg^{-1}
Specific humidity	q_a	(−)
Saturated specific humidity at T_s	q_s	(−)

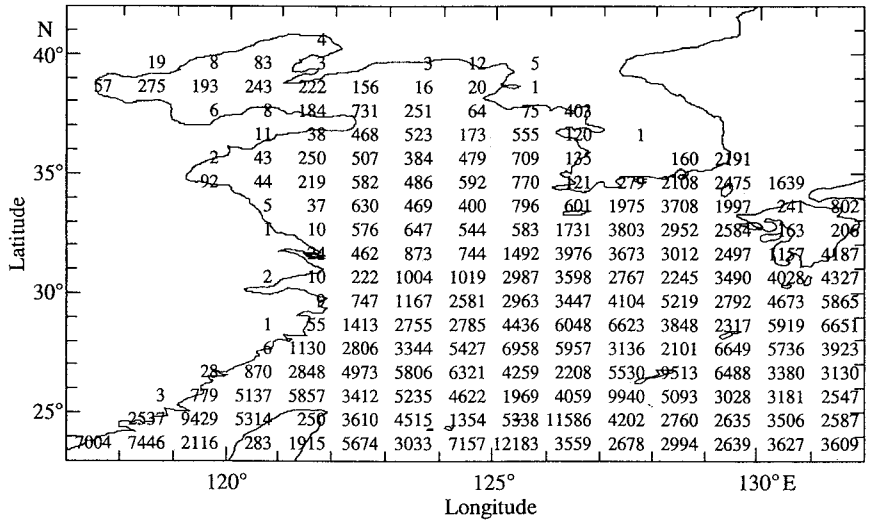

FIG. 2. Number of qualified data in each 1° square during 1960–90. The method of qualification is mentioned in section 2.

mean are eliminated in each 1° square and each month.

5) The same procedure as in step 4 is repeated with 2.5 times the new standard deviation.

Heat fluxes are then calculated at individual observation points. Monthly mean (total 372 months) interpolated values are obtained in every 1° square using a Gaussian filter with a horizontal *e*-folding scale of 100 km. If there are less than three observations inside a circle with a 100-km radius, it is regarded as a grid of missing data.

The 31-yr mean values are calculated, and N_m is introduced for each grid as the total number of months in which a monthly mean heat flux can be obtained by the interpolation method defined above. If the heat flux data is obtained on a grid every year, N_m must be 31 at a climatological month. The minimum value is 0. The long-term mean value on a grid is calculated by a simple averaging method in the case of $N_m \geq 3$ ($N_m \geq 1$ in winter). But in the case of $N_m < 3$ ($N_m = 0$ in winter), it is obtained by spline interpolation/extrapolation from the values in the adjacent area. The long-term mean field of the heat flux is calculated for every month finally.

As mentioned above, the sampling method is employed for this study. It is generally believed that the sampling method gives more accurate values than the scalar averaging method because nonlinear effects in the bulk schemes cannot be expressed by the latter (Hanawa and Toba 1987).

d. Radiation flux

Spatial variations of the solar radiation (Q_s) in early summer are shown in Figs. 4a–c. The solar radiation at the top of the atmosphere is greater for the southern part than for the northern part in the study area considering the diurnal altitude. However in April to June, Q_s is larger in the YS than in the ECS due to the variation of cloudiness. As a result, the YS and ECS receive maximum insolation in May–June and July–August, respectively (Fig. 5). This July maximum in the ECS is also confirmed by direct measurements at most meteorological observatories on the Ryukyu Islands. It can be seen from Fig. 4d that the ECS and YS receive incoming radiation uniformly on the annual average. The annual mean insolation is about 147 W m^{-2} in both ECS and YS.

Table 2 shows the annual mean solar radiation observed directly by Japan Meteorological Agency (JMA) collected from a table published by National Astronomical Observatory (1993) and calculated by several authors at three points along the ECS. The two previous studies overestimate the solar radiation compared with the direct observations. The present study gives good agreement with JMA on the average of the three points. These differences might be caused by uncertainty of the estimation schemes and the inaccuracy of cloud data.

The longwave radiation (Q_b) has small spatial variation throughout the year. It changes in the range from 20 to 70 W m^{-2} in the ECS and YS seasonally. The annual mean of the longwave radiation is 45 W m^{-2} for the ECS and 47 W m^{-2} for the YS. The difference among the previous studies is relatively smaller than for the other components.

e. Turbulent flux

Figures 4e–j show the long-term monthly and annual mean spatial variation of the sensible and latent heat fluxes (Q_h and Q_e). In summer, they have small spatial variation and magnitude. Both fluxes are increasing in autumn for all the regions. The latent heat flux in the

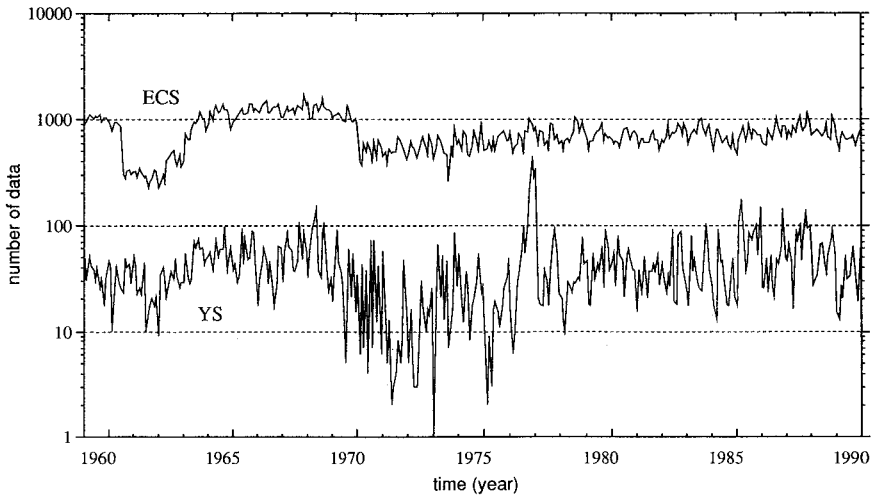

FIG. 3. Time series of the number of observations (in month) for the period from 1960 to 1990 in the study area.

YS reaches its maximum value as early as November, as shown in Fig. 5b. This may be due to the small amount of saturated vapor pressure at low air temperature in the YS during midwinter, as mentioned in Sakurai et al. (1989). In mid winter, there is a large north–south variation in the spatial distribution of the both fluxes. It can be seen from Figs. 4f,i that the sensible and latent heat fluxes have a local maximum heat loss at the eastern part of the study basin in winter due to large air–sea temperature difference. The annual mean sensible and latent heat fluxes are estimated to be 34 and 159 W m^{-2} in ECS and 18 and 72 W m^{-2} in the YS, respectively.

Figure 6a shows the comparison of the annual mean turbulent flux ($Q_h + Q_e$) obtained from some recent studies at the three positions indicated in Fig. 1. All of them were calculated using the bulk method, but the bulk coefficients and data used are different among these studies. There are serious differences especially at position C in the Kuroshio. Our result seems to give one of the central values compared with the previous studies. However, it cannot be concluded which one gives the best realistic estimation without any comparison to the direct measurement of turbulent fluxes.

f. Net heat flux

Spatial variations of the net heat flux (Q_{net}) are shown in Figs. 4k–o. In summer, the ECS and YS gain heat almost uniformly as shown in Fig. 4m. Incoming solar radiation is dominant in the net heat flux in this season. The net heat flux begins to decrease in September almost everywhere. The maximum monthly heat loss occurs in December or January due to the strong upward turbulent fluxes. This large loss of heat means that the warmer water is sufficiently cooled down by the colder air in this region.

The closed contour similar to the turbulent flux appears in the eastern part of the ECS (west side of Kyushu) except during summer. This local maximum of the upward net heat flux also appears in some previous studies (Ishii and Kondo 1987; Kang et al. 1994). The strong gradient of the heat flux is formed in the northwestern part of the ECS (Figs. 4k,l). These phenomena are similar to those in the Japan Sea (Hirose et al. 1996). This position agrees with that of frontal structure in the sea. The net heat flux increases from February while keeping the horizontal gradient until May. The reverse net heat flux occurs from March in the northern part to May over the Kuroshio.

It can be seen from Fig. 4o that the strong annual loss of heat exceeding 100 W m^{-2} occurs over the Kuroshio. This indicates that much heat advected from the Tropics is lost to the atmosphere in this region. In the vicinity around the boundary between the YS and ECS, the net heat flux is larger for the western side than for the eastern side. Kondo (1976) considered the existence of a counterclockwise circulation, seeing this horizontal variation of the heat flux. As a total, the annual mean net heat flux is about -90 and 10 W m^{-2} in the ECS and YS, respectively. The heat gain in the YS is too large to be explained by the horizontal advection of heat because the sea water temperature in the ECS is usually higher than in the YS throughout the year and because the negative heat transport from rivers is not large enough to compensate for it. The heat flux in the YS may be overestimated in this study.

Accuracy of the heat flux estimation never has been mentioned because many kinds of errors are included in the present estimation: measurement errors, database errors (cf. Lander and Morrissey 1987), uncertainties of the empirical bulk schemes, randam errors due to the small number of observations, and so on. Instead of directly estimating such complicated and unknown er-

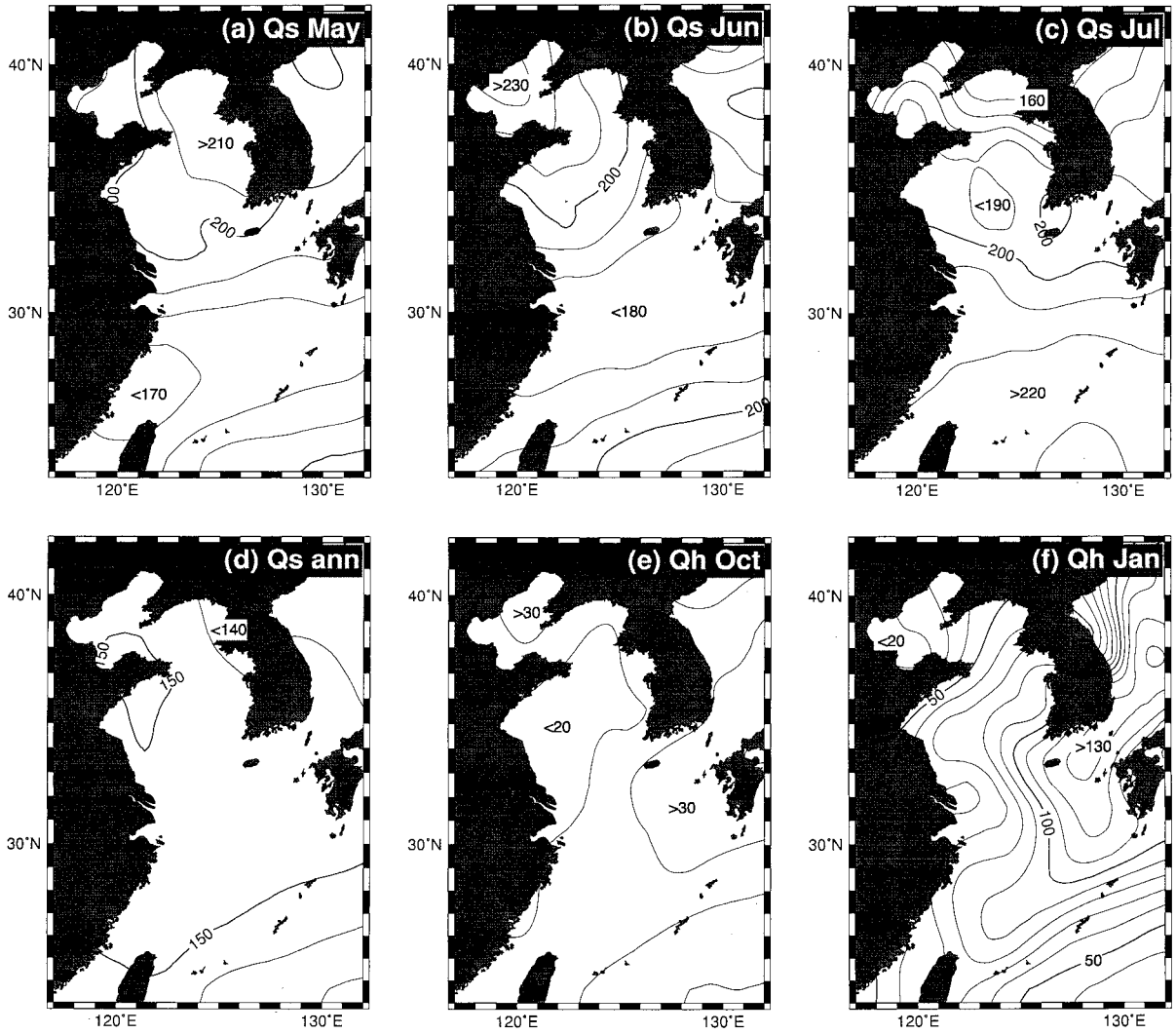

FIG. 4. Climatological monthly and annual mean spatial distributions of the net heat flux. Unit is in watts per square meter. Contour interval is 10 W m^{-2} for Q_s, Q_h and 20 W m^{-2} for Q_e, Q_{net}.

rors, the comparisons in Fig. 6 may indicate the uncertainties of the heat flux estimation in this area. The differences among these studies are roughly 20~30 and 30~50 W m^{-2} in the annual and winter mean net heat fluxes, respectively. Our result agrees with the previous studies on the whole. We can consider the accuracy of these studies should be similar to these differences.

g. Heat flux of Haney type

The Haney-type heat flux is discussed in this subsection. The quantities Q_1 and Q_2 are calculated for every $1^\circ \times 1^\circ$ grid and climatological month by the same process as described in section 2c. The net heat flux is reconstructed from (7) using the climatological monthly mean Q_1, Q_2, T_a, and T_s. We will make some comparisons of the net heat flux calculated by the bulk method and Haney type in order to examine the efficiency of the Haney type.

Figure 7a shows the monthly mean spatial variation of the net heat flux (Q_{net}) for January reconstructed by the use of (7). This distribution should be compared with Fig. 4k. These distributions must be similar to each other as long as the Haney-type condition approximates the bulk schemes. However, the Haney-type heat flux (Fig. 7a) is smaller than the net heat flux (Fig. 4k) for all of the region.

Figure 8a shows the scatter diagram of the monthly mean net heat flux calculated by the bulk method versus that by the Haney-type method. As shown in this figure, the Haney-type heat flux has enough linear relationship with the bulk method (the correlation coefficient is higher than 0.99). But the bias and rms between them is considerably large in the case of large heat loss. It is

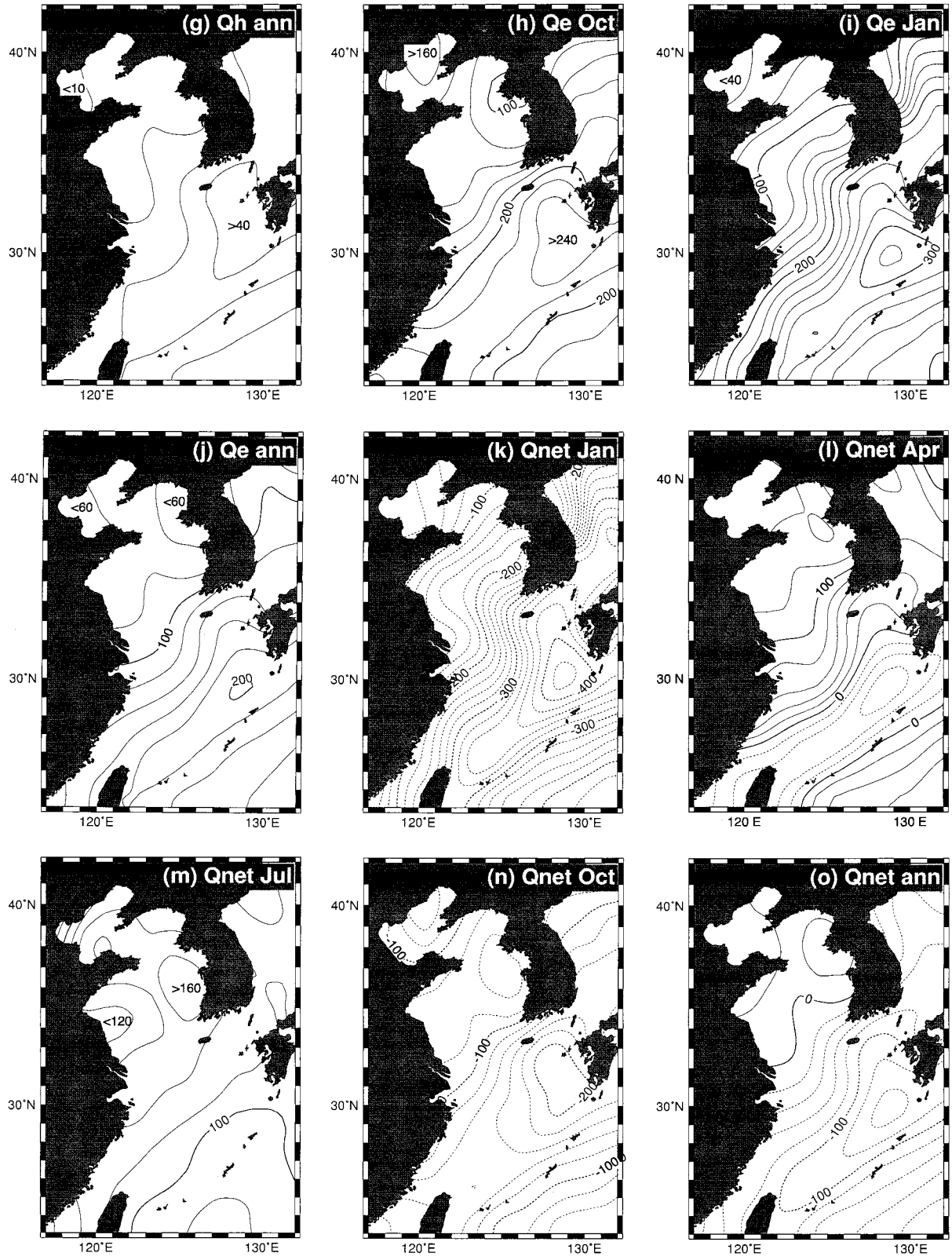

FIG. 4 (*Continued*)

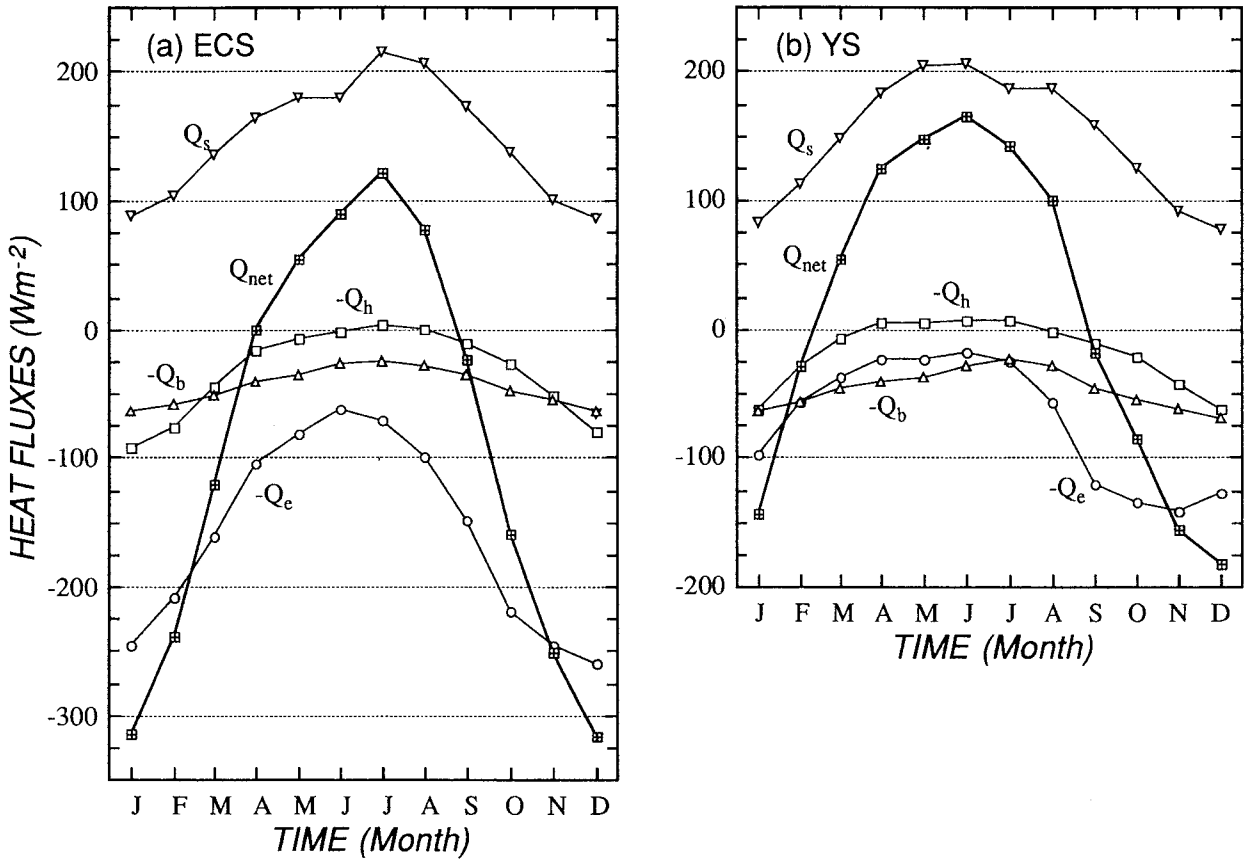

FIG. 5. Seasonal variation of the areal-mean heat fluxes for (a) ECS and (b) YS. Unit is watts per square meter.

expected that these quantities, Q_1 and Q_2, will give weaker upward heat flux and higher sea surface temperature (T_s) in numerical models.

In order to examine the reason why these disparities occurred, we compare the heat flux calculated by the bulk method and Haney type to the individual observations in Fig. 9a. It is found that the error of the net heat flux is large, especially in the case of large heat loss. We found that, if the term $(\partial Q_e/\partial T_s)_{T_a}$ is replaced by $(\partial Q_e/\partial T_s)_{(T_a+T_{obs})/2}$ in (9), a much better relation is obtained, as shown in Fig. 9b. Here, T_{obs} is the observed sea surface temperature. The truncated higher order Taylor expansion may produce this disparity. Especially, the latent heat flux depends on the temperature quadratically. Another correction method is to add the quadratic term $Q_3(T_a - T_s)^2$ to (7). This way, however, requires larger computational storage. We adopt the former method to correct the truncation error of (6).

The monthly bias between them is improved from 21.8 to 17.4 (25.6 to 19.9 W m^{-2} in rms) after the previous truncation correction as shown in Fig. 8b. The difference that still exists may occur from the difference of the averaging methods. The average of nonlinear term in (7) can be obtained by

$$\overline{Q_2(T_a - T_s)} = \overline{Q_2}(\overline{T_a} - \overline{T_s}) + \overline{Q_2'(T_a' - T_s')}. \quad (11)$$

The correct average is established by the sampling method as the left hand side of (11). Because the Haney (1971) method only gives the average of first part of the right-hand side, that is, scalar averaging method, the averaged perturbation term $\overline{Q_2'(T_a' - T_s')}$ has been ignored.

According to Hanawa and Toba (1987), because the difference between the sampling method and the scalar averaging method in the heat flux calculation is systematic, the heat flux by the scalar averaging method can be linearly transferred to that by the sampling method.

TABLE 2. Annual mean of the solar radiation (in W m^{-2}) observed at three stations: Izuhara, Naze, and Ishigaki Island. Archives by JMA dated back to 1974. Kang et al. (1994) used the NASA satellite data calculated by Pinker and Laszlo (1992). Other studies calculated the insolation by using empirical formulas and the cloud data. Kim (1992) used the cloud data observed by the satellite. Other data are essentially based on ship reports.

Authors	Period	Izuhara	Naze	Ishigaki Island
JMA	1974–90	146	133	174
Kim (1992)	1962–88	172	169	178
Kang et al. (1994)	1985–87	174	202	—
Present study	1960–90	145	147	157

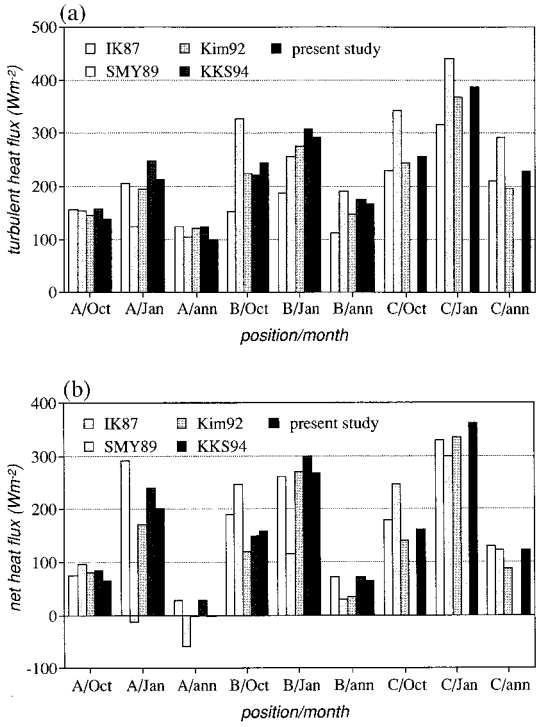

FIG. 6. Comparison of (a) turbulent flux and (b) net heat flux obtained from the several authors on October, January, and the annual mean at the three positions A, B, and C indicated in Fig. 1: IK87, SMY89, Kim92, and KKS94 stand for Ishii and Kondo (1987), Sakurai et al. (1989), Kim (1992), and Kang et al. (1994), respectively.

Based on their idea, the *improved* quantities Q_1^* and Q_2^* are obtained through least squares fitting,

$$Q_1^* = Q_1^{tc} - 12.731 \tag{12}$$

$$Q_2^* = 1.0569 Q_2^{tc}, \tag{13}$$

where superscripts * and *tc* denote the improved and the truncation-*corrected* quantities of the Haney type, respectively. The result is shown in Fig. 8c. The bias between the bulk method and Haney type becomes approximately zero. The monthly mean distribution of the net heat flux (Q_{net}) for January reconstructed by the improved Haney type is shown in Fig. 7b. The disparity in the distribution of Q_{net} with Fig. 4k is hardly visible. It can be concluded that the improved heat flux of Haney type has enough accuracy to estimate the monthly mean net heat flux.

As we can see in Fig. 10, the quantity Q_2^* is 1.2 to 1.5 times larger than Q_2 in the cooling season: Q_2^* is expected to give stronger upward heat transport through the sea surface than Q_2 in winter. Also Q_2^* has larger spatial variation than Q_2 (Fig. 11); Q_1 and Q_1^* have also a strong spatial and temporal variation. They attain their maximum in July and June and minimum in December, as shown in Fig. 10. The annual averages of the quantities Q_1^* (Q_1) and Q_2^* (Q_2) are 4.8 (17.5) and 49.5 (45.2) W m^{-2} °C^{-1} in the ECS and 43.2 (55.9) and 31.0 (27.6) W m^{-2} °C^{-1} in the YS, respectively.

3. Numerical model

In order to examine the efficiency of the improved Haney type (Q_1^* and Q_2^*) and to obtain the more rea-

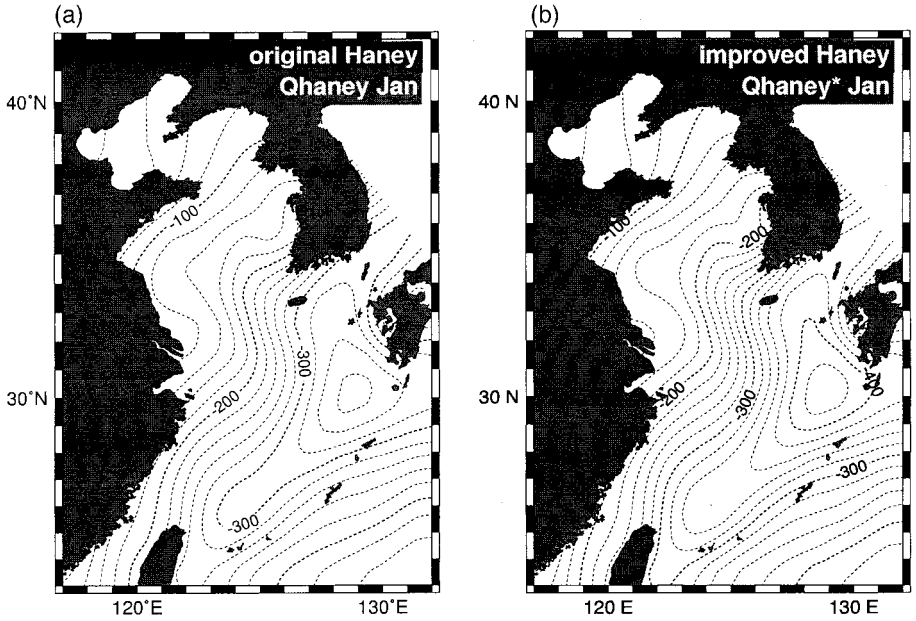

FIG. 7. Climatological monthly mean spatial variation of the net heat flux for January reconstructed by the use of (7) using climatological monthly mean T_a, T_s: (a) Q_1, Q_2 and (b) Q_1^*, Q_2^*.

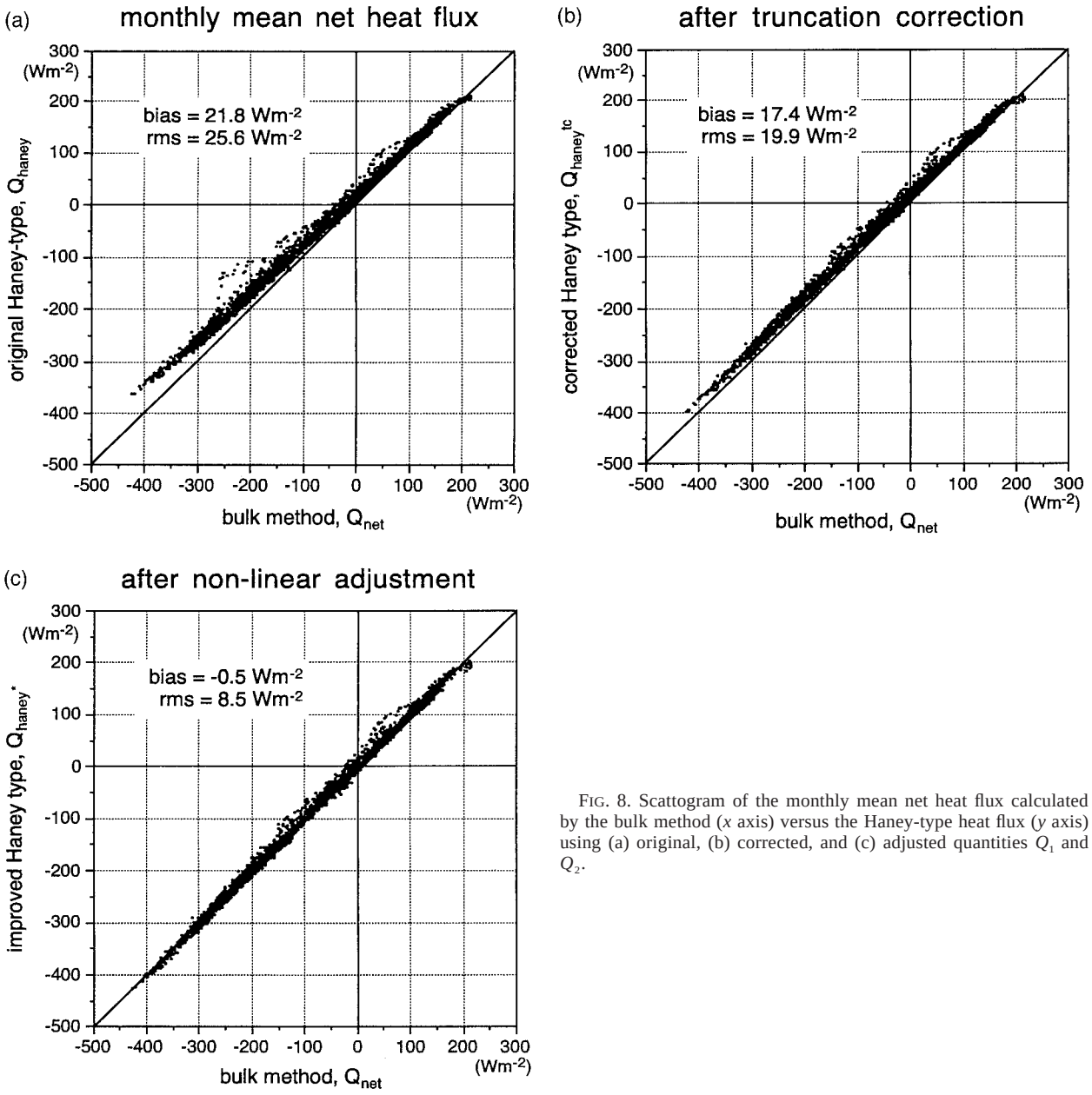

FIG. 8. Scattogram of the monthly mean net heat flux calculated by the bulk method (x axis) versus the Haney-type heat flux (y axis) using (a) original, (b) corrected, and (c) adjusted quantities Q_1 and Q_2.

sonable heat flux in the YS, a numerical simulation for the study area is carried out with the *original* and the *improved* Haney-type surface thermal boundary conditions.

a. Model characteristics

The numerical ocean model originally constructed at the Research Institute for Applied Mechanics in Kyushu University, RIAMOM, is used for this study. RIAMOM is a z-coordinate primitive OGCM developed by Lee (1996).

The generalized Arakawa scheme, which conserves both potential energy and enstrophy (Mesinger and Arakawa 1976), is applied for the advection term of the horizontal momentum equations in order to prevent nonlinear instability, which may happen through the long-term integration. This scheme is vectorized by the method of Ishizaki and Motoi (1999, manuscript submitted to *J. Atmos. Oceanic Technol.*). The so-called *slant advection* effect (Takano 1978; Ohnishi 1978) is adopted to correctly represent the vertical advection of the horizontal momentum along steep bottom topography.

RIAMOM has a free surface that allows external gravity waves. The external gravity waves require much smaller time steps, especially for the deep ocean. A

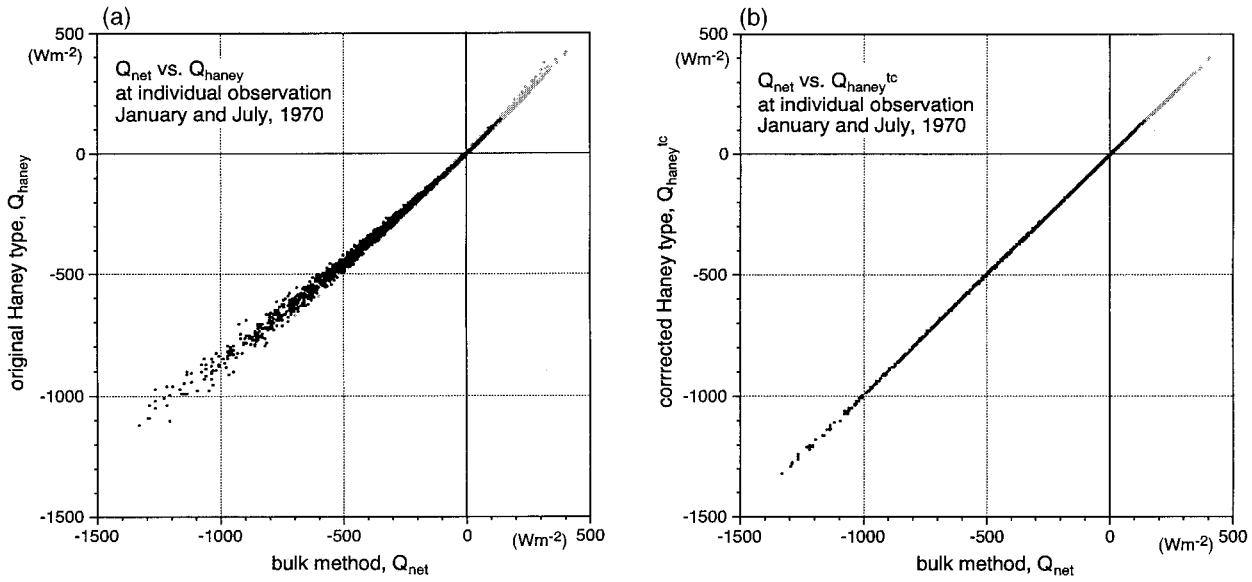

FIG. 9. Scattogram of the net heat flux at the individual observation calculated by the bulk method (x axis) versus the Haney-type heat flux (y axis) using (a) original, and (b) corrected quantities Q_1 and Q_2 for January and July 1970.

mode splitting method is adopted to avoid this problem, that is, the governing equation is divided into vertical integrated and structure equations (Blumberg and Mellor 1987). The time integration is executed by a leapfrog scheme using the Euler backward scheme intermittently. The barotropic and baroclinic time steps are taken as 30 and 1800 s, considering the CFL condition in this study. Details of RIAMOM are given in Lee (1996).

b. Model conditions

Twenty levels at each standard CTD observation level are vertically prepared in this model as shown in Table 3. Realistic bottom topography is given by ETOPO5 with the deepest bottom of 1500 m. The horizontal resolution is $\frac{1}{5}^\circ$ for both latitude and longitude. The horizontal and vertical eddy viscosities are the constants 4×10^6 and 1.0 $cm^2\ s^{-1}$, respectively. The horizontal eddy diffusivity is set to be 3×10^6 $cm^2\ s^{-1}$. The Munk and Anderson (1948) scheme, which has tidal and turbulent mixing terms, is applied for the vertical eddy diffusivity to represent the strong tidal variability in the ECS and YS.

The model basin has five horizontal open boundaries as shown in Fig. 12. Three are for inflow (the strait east of Taiwan, the Taiwan Strait, and the Yangtze/Changjang River) and two are for outflow (the Tsushima/Korea Straits and Tokara Strait). Volume transport through

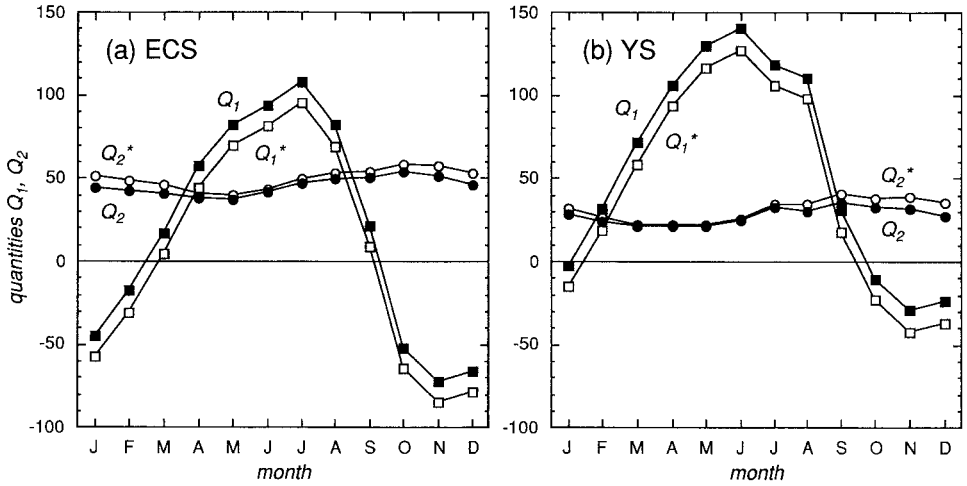

FIG. 10. Seasonal variation of the areally averaged quantities Q_1 and Q_2 of Haney type for (a) ECS and (b) YS. The unit is in W m^{-2} for Q_1 and W m^{-2} °C^{-1} for Q_2.

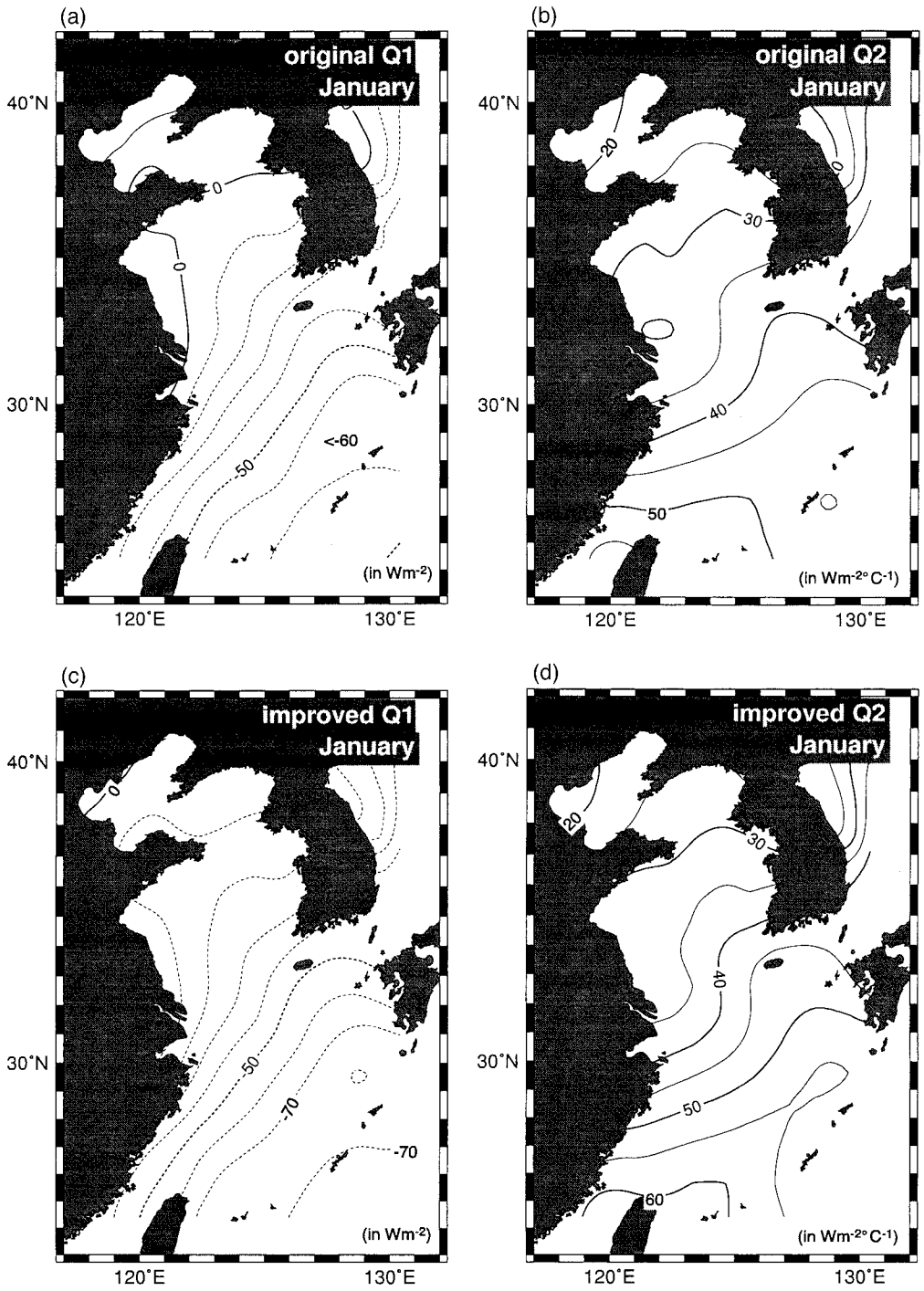

FIG. 11. Climatological monthly mean distribution of the quantities Q_1 and Q_2 of the Haney-type condition: (a), (b) original type and (c), (d) improved type.

TABLE 3. Vertical resolution of the numerical simulation. Layer thickness and depth are in meters.

Level	1	⋯	3	4	5	⋯	8	9	⋯	11	12	⋯	18	19	20
Thickness	10	⋯	10	20	25	⋯	25	50	⋯	50	100	⋯	100	250	250
Depth	10	⋯	30	50	75	⋯	150	200	⋯	300	400	⋯	1000	1250	1500

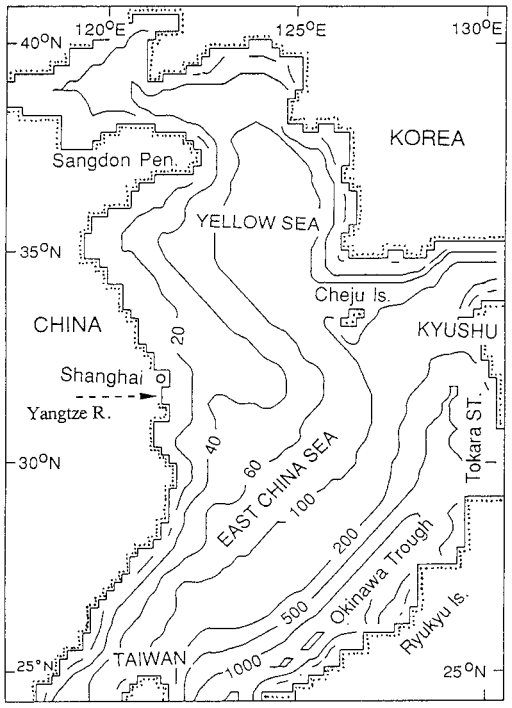

FIG. 12. Model basin. The model has three openings (Yangtze/Changjang River, east and west of Taiwan) for inflow and two channels (Tokara and Tsushima/Korea Straits) for outflow.

these openings is defined by the recent measurements as shown in Table 4. The inflows though the Taiwan Strait and Yangtze River and the outflow through the Tsushima/Korea Straits are assumed to have sinusoidal seasonal variation. The flow through the Ryukyu Islands is assumed to be negligible except for the Kuroshio.

The vertical distributions of the temperature and salinity at the strait east of Taiwan and the Taiwan Strait are given by the seasonal dataset of Levitus (1982). The climatological monthly mean data is interpolated into the model resolution in time and space. The barotropic velocities normal to each section are assumed to be horizontally uniform, and the baroclinic velocities are computed by the thermal wind balance. Five grids (= 1°) near the open boundaries are wasted as sponge layers: the viscosity is linearly increased by a factor of 5. A nonslip condition is applied for both topographic and open boundaries.

The 10-yr monthly mean wind stress field over the model basin is given by Na et al. (1992). The surface heat flux is given by the two kinds of Haney-type condition calculated in the previous section.

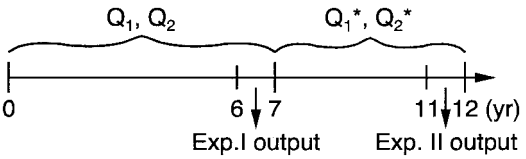

FIG. 13. Two experiments are carried out by running a simulation for 12 years starting from rest. The model is driven by the original heat flux of Haney (1971) type for the first 7 years, and by the improved type for the last 5 years.

The two experiments are carried out by running a simulation for 12 years starting from rest considering spinup time as shown in Fig. 13. In experiment I (year 1 to 7), the quantities Q_1 and Q_2 are used as the original Haney type, while in Experiment II (year 8 to 12), the improved Haney-type heat flux, Q_1^* and Q_2^*, are applied to the surface thermal boundary condition. The same climatological monthly mean air-temperature field is used as for the previous section. The sea surface temperature T_s is replaced by the water temperature at the first level in the model.

Salinities at the shallowest level are restored to the climatological seasonal mean fields (Levitus 1982) with 30 days damping time. The initial conditions of temperature and salinity are given by the winter fields of Levitus data. The fields for year 7 and 12 will be discussed in the next subsection.

c. Results

Figure 14 shows the spatial distributions of the net heat flux for the January and annual means simulated in the both experiments. The annual-mean net heat flux in the two experiments is -60.0 and -23.6 W m^{-2} in the ECS and -39.4 and -43.0 W m^{-2} in the YS, respectively. The vigorous upward heat flux occurs using the improved type (expt II) in the YS but is weaker using the original type. The two distributions are similar to the result from data analysis (Figs. 4k,o) except over the Kuroshio region. The inflow temperature condition might be underestimated due to the large-scale filtering of Levitus (1982), and the upward heat flux might be weakened over the Kuroshio region in the process of restoring the sea surface temperature to the air temperature.

TABLE 4. Volume transport conditions at the openings given in this study. The positive values indicate the inflow condition.

Opening	Transport (Sv)	Date of maximum	Source
East of Taiwan	23	No variation	Takematsu et al. (1986) Chen et al. (1992) Ichikawa and Beardsley (1993)
Taiwan Strait	1.5 ± 0.5	15 Aug	Zhao and Fang (1991)
Yangtze River	0.03 ± 0.015	15 Aug	Beardsley et al. (1985)
Tsushima–Korea Straits	−2.3 ± 0.35	15 Sep	Isobe (1994a,b)
Tokara Strait	Residual		

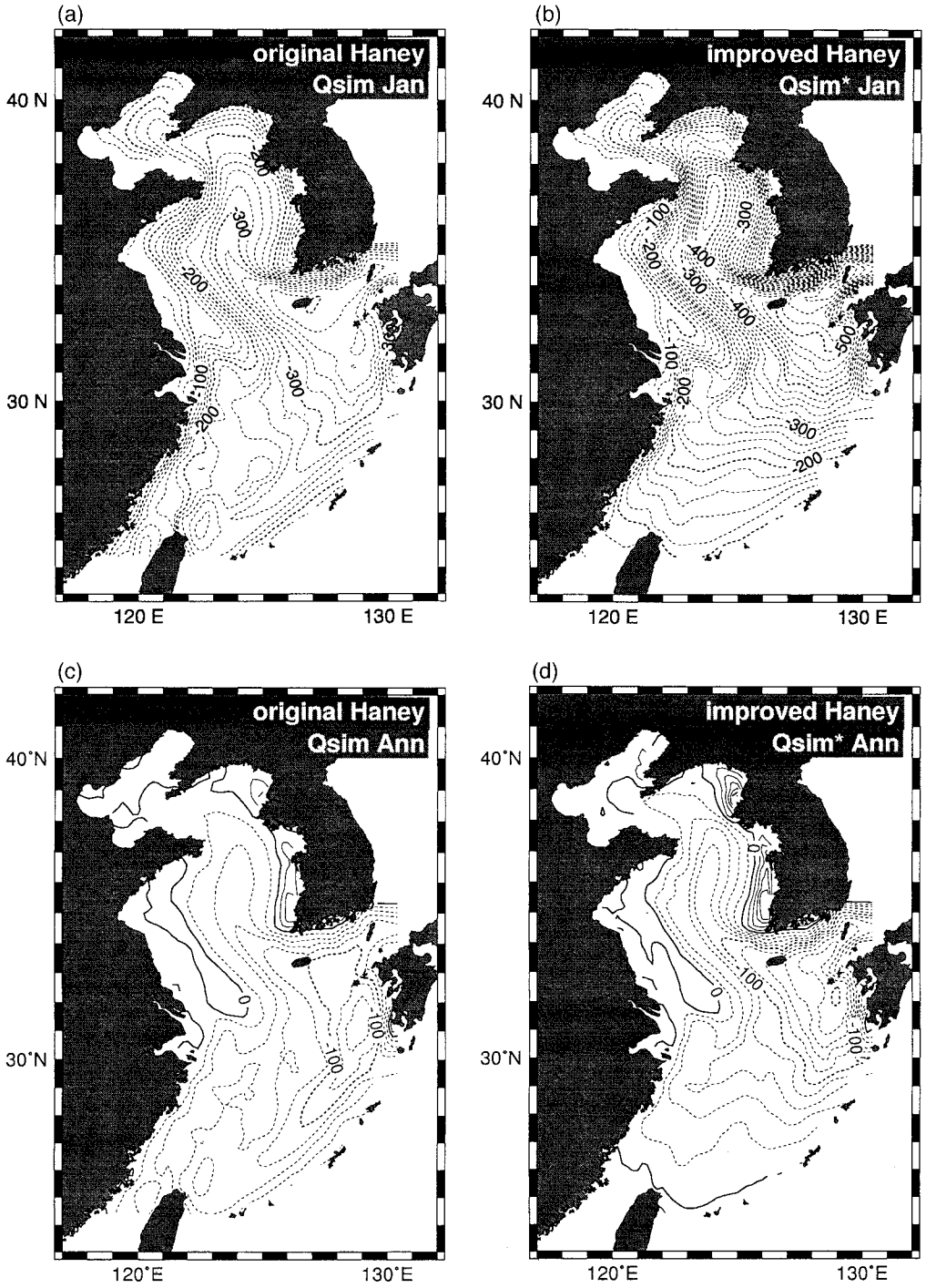

FIG. 14. Spatial distribution of the net heat flux for January and the annual mean by the both original and improved heat flux of Haney type.

The local variation could not be discussed in the previous data analysis because of the large-scale spatial filtering (~100 km) due to the limitation of the amount of data. A tongue-shaped contour simulated in the central part of YS indicates the warm water flowing from the south. At the coastal region northeast of the Yangtze River mouth, another tongue-shaped contour can be found. A strong winter monsoon may form the vertically homogeneous cold water in the shallow water region.

As discussed in section 2f, the net heat flux seemed to be overestimated in the YS by the analysis in terms of the total heat budget of the sea. The annual mean

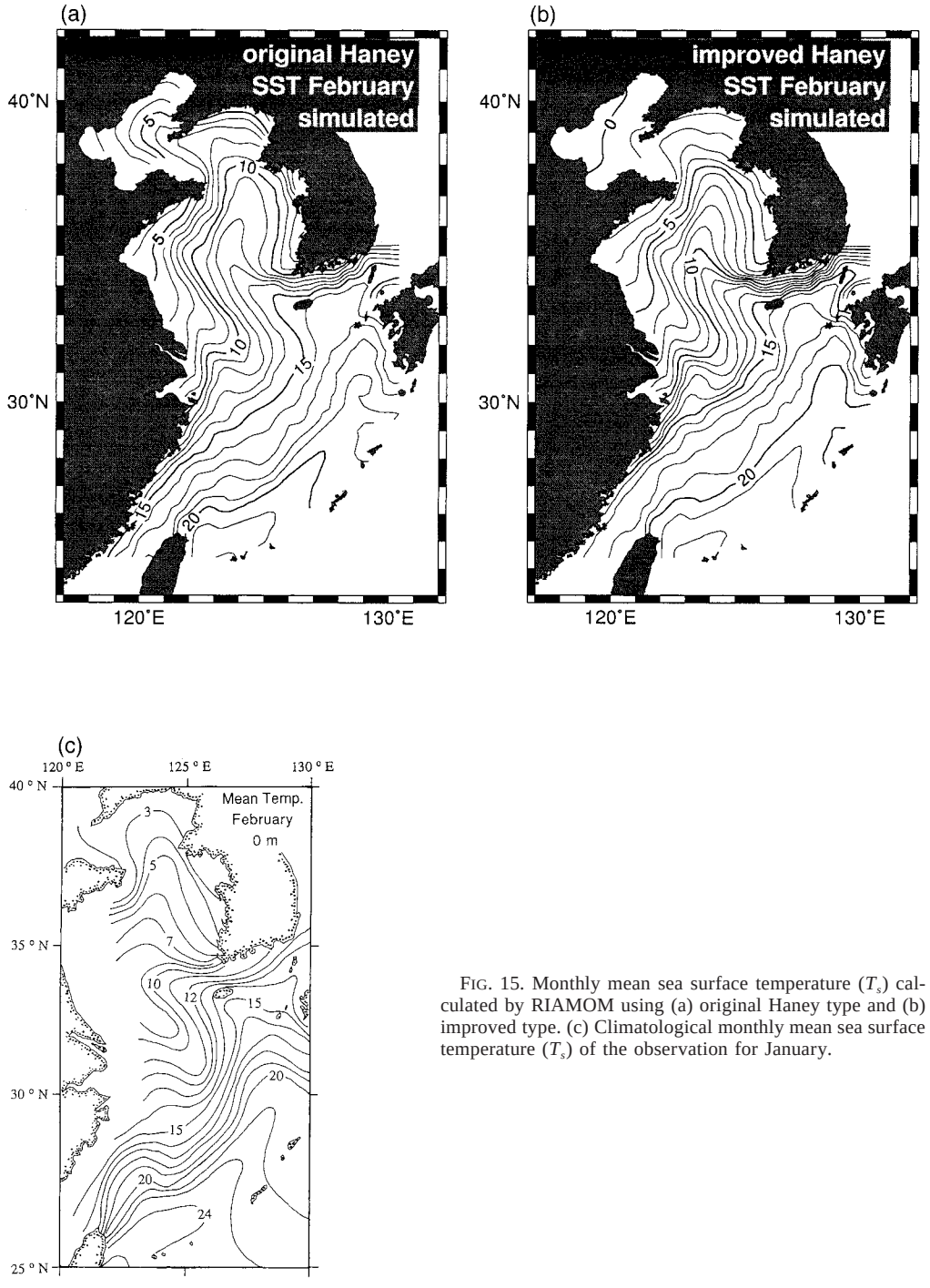

FIG. 15. Monthly mean sea surface temperature (T_s) calculated by RIAMOM using (a) original Haney type and (b) improved type. (c) Climatological monthly mean sea surface temperature (T_s) of the observation for January.

surface heat flux in the YS is negative in both experiments (i.e., the sea loses heat to the atmosphere), and it is balanced by heat advection–diffusion from the ECS for heat conservation in the model. The simulated heat flux in the YS is more reasonable in this sense.

The three distributions of sea surface temperature in winter are shown in Fig. 15. Figures 15a,b show the monthly mean distributions of T_s simulated by RIAMOM. Figure 15c is obtained from JODC (1978). The three fields are qualitatively similar but quantitatively different. The simulated T_s in experiment II is more similar to the observed one than in experiment I. A remarkable difference between the two experiments is found in the YS due to the stronger heat loss in experiment II. The temperature simulated near the inflow of the Kuroshio east of Taiwan is about 2°C lower than the observation,

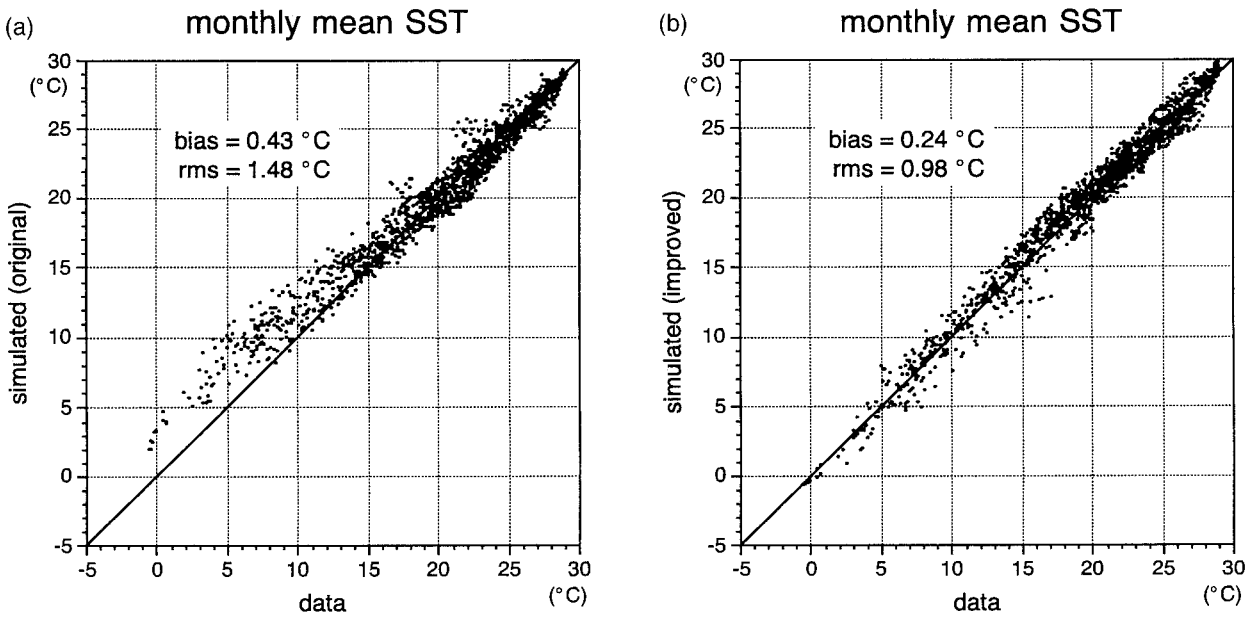

FIG. 16. Scatter diagram of T_s analyzed by using the observation data versus simulated by (a) original Haney type and (b) improved Haney type, respectively.

which supports the underestimated inlet temperature, as previously discussed.

Comparisons of T_s calculated by the analysis and by simulation are shown in Fig. 16. We can immediately find higher sea surface temperature simulated by the original Haney-type condition under 15°C compared to the in situ observation. The rms difference of T_s between the data analysis and the numerical model is 1.48°C in experiment I and 0.98°C in experiment II. This comparative experiment demonstrates the improvement of the Haney-type formulation for the real field in terms of the sea surface temperature simulation.

The water temperatures in the subsurface levels are also improved in the improved Haney-type formulation (H.-C. Lee and J.-H. Yoon 1997, unpublished manuscript).

4. Summary and discussions

The long-term monthly mean surface heat fluxes over the ECS and YS have been calculated by both the bulk method and the RIAMOM. The heat fluxes estimated by the bulk method were compared with the direct observation of solar radiation and to previous studies. The heat flux estimated in this study may be more realistic compared to previous studies in the ECS, while the heat gain in the YS seems to be overestimated. The uncertainty of the estimation schemes and/or the scarcity of the observation might cause this overestimation. Actually, the empirical formulas used in this study are reliable only in the neighboring seas around Japan (Kim and Kimura 1995). However, these schemes are not assured in areas away from Japan.

The numerical experiments for the study area were also carried out by using the Haney-type heat flux as the surface thermal boundary condition. The quantities Q_1 and Q_2 of the Haney type were also calculated in this study. Some corrections were proposed because the net heat flux reconstructed using the original Haney type overestimated the net heat flux, that is, gave weaker upward heat flux, compared to that calculated by the bulk method. It was demonstrated that the improved Haney type gave the more realistic sea surface temperature than the original Haney type in the study region compared with the observation.

Concerning the heat flux condition of Barnier et al. (1995), similar perturbation terms as (11) are neglected also in their formation. A correction may be required in order to evaluate a more accurate damping coefficient. The averaged perturbation term is expected to be smaller and negligible in their formation because their restoring quantity (sea surface temperature) changes much slower than the Haney restoring quantity (air temperature).

The annual mean net heat flux in the YS was simulated to be negative in both experiments. This means that surface heat flux consistent with the heat budget in the YS should be negative. This may be easily understood by thinking that the YS is always colder than the ECS and that the horizontal heat transport from the ECS to YS should be positive. In this sense, the net heat flux calculated by RIAMOM in the YS is more reasonable than by the present data analysis.

Acknowledgments. The authors would like to express our special thanks to Proffesor A. G. Ostrovskii, Dr. C.-H. Kim, and Mr. T. Kondo (Kyushu University) for their useful discussions and comments. Dr. Ishii and Dr. Sak-

urai kindly provided us their heat flux data for comparison. We are also grateful to JMA and JODC for offering data files. The heat flux data analyzed in this study is available to anyone via anonymous ftp > 133.5.179.158.

REFERENCES

Barnier, B., L. Siefridt, and P. Marchesiello, 1995: Thermal forcing for a global ocean circulation model using a three-year climatology of ECMWF analysis. *J. Mar. Syst.,* **6,** 363–380.

Beardsley, R., R. Limeburner, H. Yu, and G. A. Cannon, 1985: Discharge of the Chanjang (Yangtze River) into the East China Sea. *Contin. Shelf Res.,* **4,** 57–76.

Berliand, M. E., and T. G. Berliand, 1952: Determining the net longwave radiation of the earth with consideration of the effect of cloudiness (in Russian). *Izv. Akad. Nauk. USSR Ser. Geofiz.,* No. 1, 64–78.

Blumberg, A. F., and G. L. Mellor, 1987: A description of a three-dimensional coastal ocean circulation model. *Coastal and Estuarine Sciences 4,* N. S. Heaps, Ed., Amer. Geophys. Union, 1–16.

Chen, C., R. C. Beardsley, and R. Limeburner, 1992: The structure of the Kuroshio southeast of Kyushu: Velocity, transport and potential vorticity fields. *Deep-Sea Res.,* **39,** 245–268.

Efimova, N. A., 1961: On methods of calculating monthly values of net longwave radiation (in Russian). *Meteor. Gidrol.,* **10,** 28–33.

Hanawa, K., and Y. Toba, 1987: Critical examination of estimation methods of long-term mean air–sea heat and momentum transfers. *Ocean–Air Interact.,* **1,** 79–93.

Haney, R. L., 1971: Surface thermal boundary condition for ocean circulation models. *J. Phys. Oceanogr.,* **1,** 241–248.

Hirose, N., C.-H. Kim, and J.-H. Yoon, 1996: Heat budget in the Japan Sea. *J. Oceanogr. Soc. Japan,* **52,** 553–574.

Ichikawa, H., and R. C. Beardsley, 1993: Temporal and spatial variability of volume transport of the Kuroshio in the East China Sea. *Deep-Sea Res.,* **40,** 583–605.

Ishii, T., and J. Kondo, 1987: Seasonal variation of the heat balance of the East China Sea (in Japanese). *Tenki,* **34,** 517–526.

Isobe, A., 1994a: Seasonal variability of the barotropic and baroclinic motion in the Tsushima-Korea Strait. *J. Oceanogr. Soc. Japan,* **50,** 223–238.

——, 1994b: Tsushima warm current at Tsushima Straits (in Japanese). *Kaiyo Mon.,* **26,** 802–809.

JODC, 1978: *Marine Environment Atlas, Northwestern Pacific Ocean II (seasonal and monthly).* Japan Hydrographical Association, 157 pp.

Kang, I.-S., M.-K. Kim, and T. Shim, 1994: Seasonal variation of surface heat budget and wind stress over the seas around the Korean peninsula (in Korean with English abstract). *J. Korean Soc. Oceanogr.,* **29,** 325–337.

Kim, Y.-S., 1992: Estimate of heat transport across the sea surface near Japan with bulk methods. Ph.D. thesis, University of Tokyo, 124 pp. [Available from University of Tokyo Library, 7-3-1 Hongo Bunkyo-ku, Tokyo 113-8654, Japan.]

——, and R. Kimura, 1995: Error evaluation of the bulk aerodynamic method for estimating heat flux over the sea. *J. Korean Meteor. Soc.,* **31,** 399–413.

Kondo, J., 1975: Air–sea bulk transfer coefficients in diabatic conditions. *Bound.-Layer Meteor.,* **9,** 91–112.

——, 1976: Heat balance of the East China Sea during the Air Mass Transformation Experiment. *J. Meteor. Soc. Japan,* **54,** 382–398.

Lander, M. A., and M. I. Morrissey, 1987: Unexpected duplicate ship reports in the Comprehensive Ocean–Atmosphere Data Set (COADS). *Trop. Ocean–Atmos. Newslett.,* **38,** 13–14.

Lee, H.-C., 1996: A numerical simulation for the water masses and circulations in the Yellow Sea and the East China Sea. Ph.D. thesis, Kyushu University, 150 pp. [Available from Kyushi University Library, 6-10-1 Hakozaki Higashi-ku, Fukuoka 812-8581, Japan.]

Levitus, S., 1982: *Climatological Atlas of the World Ocean.* NOAA Prof. Paper No. 13, U.S. Govt. Printing Office, Washington DC, 173 pp. [Available from U.S. Government Printing Office, Washington, DC 20402.]

Mesinger, F., and A. Arakawa, 1976: *Numerical Methods Used in Atmospheric Models.* GARP Publ. Series No. 17, Vol 1, WMO–ICSU Joint Organizing Committee, 64 pp.

Munk, W. H., and E. R. Anderson, 1948: Notes on a theory of the thermocline. *J. Mar. Res.,* **7,** 276–295.

Na, J. Y., J. W. Seo, and S. K. Han, 1992: Monthly-mean sea surface winds over the adjacent seas of the Korean Peninsula (in Korean with English abstract). *J. Oceanogr. Soc. Korea,* **27,** 1–10.

National Astronomical Observatory, 1993: Rika nenpyo (Chronological Scientific Tables) 1994 (in Japanese). Vol. 67, Maruzen Co., 1042 pp.

Ohnishi, Y., 1978: Method of numerical studies: Marginal seas (in Japanese). *Oceanography as Environmental Science,* S. Horibe, Ed., University of Tokyo Press, 246–271.

Pinker, R. T., and I. Laszlo, 1992: Modeling surface irradiance for satellite applications on a global scale. *J. Appl. Meteor.,* **31,** 194–211.

Reed, R. K., 1977: On estimating insolation over the ocean. *J. Phys. Oceanogr.,* **7,** 482–485.

Sakurai, M., A. Maeda, and T. Yamashiro, 1989: Sea surface heat exchange and water budget in the Yellow Sea and the East China Sea (in Japanese). *Kaiyo Mon.,* **21,** 412–415.

Seckel, G. R., and F. H. Beaudry, 1973: The radiation from sun and sky over the North Pacific Ocean (abstract). *Trans. Amer. Geophys. Union,* **54,** 1114.

Takano, K., 1978: The effect of the ridge on the circulation of the deep and bottom layer (in Japanese). *Oceanography as Environmental Science,* S. Horibe, Ed., University of Tokyo Press, 27–44.

Takematsu, M., K. Kawatate, W. Koterayama, T. Suhara, and H. Mitsuyasu, 1986: Moored instrument observations in the Kuroshio south of Kyushu. *J. Oceanogr. Soc. Japan,* **42,** 201–211.

Zhao, B., and G. Fang, 1991: The estimate of transport of the main water route in the East China Sea. *Acta Oceanol. Sin.,* **B** (2), 169–178.